

Journal Homepage: www.journalijar.com

INTERNATIONAL JOURNAL OF ADVANCED RESEARCH (IJAR)

Article DOI: 10.21474/IJAR01/22377

DOI URL: <http://dx.doi.org/10.21474/IJAR01/22377>

RESEARCH ARTICLE

EVALUATING THE PARFLOW-CLM INTEGRATED MODEL IN ONE DIMENSION: REVISITING WATER AND ENERGY BUDGETS IN THE CULTIVATED SAHEL (WANKAMA, NIGER)

Mahamadi Tabsoba^{1,2}

1. Univ. Grenoble Alpes, IRD, CNRS, INRAE, Grenoble INP, IGE, 38000 Grenoble, France.

2. Univ. Abomey-Calavi, Doctoral School of Agricultural and Water Sciences, Cotonou 01 BP 526, Benin.

Manuscript Info

Manuscript History

Received: 8 October 2025

Final Accepted: 10 November 2025

Published: December 2025

Key words:-

ParFlow-CLM, Hydrological modeling,
Water balance, semi-arid ecosystems,
Sahel.

Abstract

This study evaluates the integrated hydrological model Par Flow–CLM (PF-CLM) in a 1-D configuration over two Sahelian agro-ecosystems (rainfed millet and fallow bush) at Wankama, Niger, using 2006–2011 in-situ forcing and observations data. The soil column is discretized into five horizons with a crusted surface layer; key hydraulic (K_s , α , n) and radiative (albedo) parameters are calibrated via Latin Hypercube sampling against evapotranspiration onset, runoff coefficients, and albedo dynamics. Kling-Gupta Efficient (KGE), correlation, and Nash–Sutcliffe efficiency (NSE) are used to evaluate model performance. The results showed that PF-CLM reproduces surface energy fluxes with good skill ($KGE \approx 0.75$ – 0.80 for R_n and LE) and captures seasonal wetting–drying cycles in near-surface soil moisture ($KGE \approx 0.65$ – 0.81 at 10–50 cm), with performance decreasing at depth, especially under fallow. Annual water budgets are realistic: evapotranspiration accounts on average for ~82% (millet) and ~88% (fallow) of rainfall; runoff represents ~16% and ~13%, and deep drainage is negligible to slightly negative (≈ 0 to -2% of P). ParFlow–CLM produces higher runoff, slightly lower evaporation, and limited but non-zero vertical redistribution within the soil profile, rather than effective downward percolation. These results support the use of PF-CLM for process studies and for scaling to 2-D hillslopes to assess sustainable land-management impacts on infiltration–runoff partitioning and recharge in the Sahel.

"© 2025 by the Author(s). Published by IJAR under CC BY 4.0. Unrestricted use allowed with credit to the author."

1 Introduction

The Sahelian region of West Africa is characterized by high climatic variability, short and intense rainy seasons, and fragile agroecosystems where rainfall partitioning largely determines water availability and agricultural productivity (Bodjrenou et al., 2025a; 2025b).

Corresponding Author:-Mahamadi Tabsoba

Address:-1. Univ. Grenoble Alpes, IRD, CNRS, INRAE, Grenoble INP, IGE, 38000 Grenoble, France 2.
Univ. Abomey-Calavi, Doctoral School of Agricultural and Water Sciences, Cotonou 01 BP 526, Benin.

Understanding how rainfall is divided among evapotranspiration, runoff, and infiltration remains essential for predicting ecosystem functioning and managing soil and water resources under increasing climatic stress (Lebel et al., 2009; Descroix et al., 2018). In these semi-arid systems, soil surface conditions especially crusting and sparse vegetation cover play a decisive role in controlling infiltration and energy exchanges (Casenave & Valentin, 1992; Peugeot et al., 1997).

Over the past decades, numerous field and modeling studies have quantified the water and energy budgets of rainfed millet fields and fallow bush systems in the Sahel, notably in Niger, Mali, and northern Nigeria (Kassam & Kowal, 1975; Payne et al., 1991; Velluet et al., 2014.). These studies consistently report that evapotranspiration accounts for 80–85 % of annual rainfall, confirming its central role in the regional hydrological cycle (Velluet et al., 2014). However, the partitioning of water losses varies with land use: while millet fields combine both runoff and drainage losses, fallow systems lose water mainly through surface runoff. Energy balance analyses further indicate that evapotranspiration represents roughly 88 % of net radiation, underlining the tight coupling between hydrological and radiative processes (Kassam & Kowal, 1975).

Recent research has emphasized key limitations of conventional soil–vegetation–atmosphere transfer (SVAT) models and the need for more integrated approaches. Diongue et al. (2022) demonstrated that parameter uncertainty—particularly in soil hydraulic parameters significantly affects water balance simulations in semi-arid contexts; they found that inverse calibration in HYDRUS-1D outperforms pedotransfer approaches in the Groundnut Basin of Senegal. Similarly, Ibrahim et al. (2014) highlighted a long-term increase in diffuse groundwater recharge following agricultural expansion in the Sahel, showing that land use change can substantially modify the hydrological regime. At the groundwater–atmosphere interface, Diouf et al. (2020) modeled evapotranspiration from a shallow aquifer, demonstrating that groundwater dynamics can buffer seasonal water deficits in semi-arid systems. Finally, studies such as Ezzahar et al. (2009) and Demarty et al. (2002) have shown that remote-sensing-based calibration of SVAT models can effectively constrain surface temperature and soil moisture estimates, improving the energy balance closure.

Within this broader context, Velluet et al. (2014) established a multi-year benchmark of coupled water and energy processes in the cultivated Sahel at the Wankama site (southwestern Niger), using the one-dimensional SiSPAT model (Braud et al., 1995). Their study remains a reference for quantifying vertical fluxes in millet and fallow systems but does not capture integrated hydrological feedbacks such as lateral flow and groundwater exchange. The integrated model ParFlow–CLM (Maxwell & Miller, 2005; Maxwell et al., 2015) offers a physically based coupling between surface and subsurface hydrology and energy processes, allowing the simulation of both vertical and lateral water redistribution (Kollet & Maxwell, 2008). Recent applications in the upper Ouémé basin (Benin) have confirmed the model’s potential for reproducing surface–subsurface interactions under tropical conditions (Bodjrènou et al., 2023).

This study aims to evaluate the ability of the integrated model ParFlow–CLM to reproduce the surface energy and water budgets of Sahelian agroecosystems (rainfed millet and fallow bush) under 1D configuration, using the multi-year Wankama dataset. This work provides a foundation for future 2D–3D applications of ParFlow–CLM in the Sahel to explore the impacts of land management and restoration practices on hydrological processes.

2 Data and Methodology

2.1 Study area description

This study is conducted in the Wankama catchment, located in southwestern Niger (13°38' N, 2°37' E) (Figure 1.a), one of the long-term monitored sites of the AMMA-CATCH observatory (Cappelaere et al., 2009). Wankama is a small endorheic basin of approximately 2 km² connecting a lateritic plateau to hydromorphic lowlands that host three temporary ponds during the rainy season (Gendre, 2010). The catchment is also part of the Dantiandou Kori system, a network of small basins typical of the cultivated Sahel. In 2005, land use was dominated by rainfed millet fields (≈ 58%), fallow bush (≈ 23%), and bare or degraded surfaces (Peugeot et al., 2003), forming a heterogeneous landscape representative of Sahelian agroecosystems. The regional climate is semi-arid, characterized by a short monsoon season (June–September) and a long dry period.

Two experimental plots (millet field and fallow bush) (Figure 1.b) were instrumented to monitor surface–atmosphere exchanges, soil water content, and energy fluxes continuously (Cappelaere et al., 2009; Ramier et al., 2009). Surface

conditions vary seasonally and with land use. Millet fields display transient structures shaped by tillage and rainfall impact, while fallow areas exhibit persistent crusted surfaces and higher infiltration contrasts.

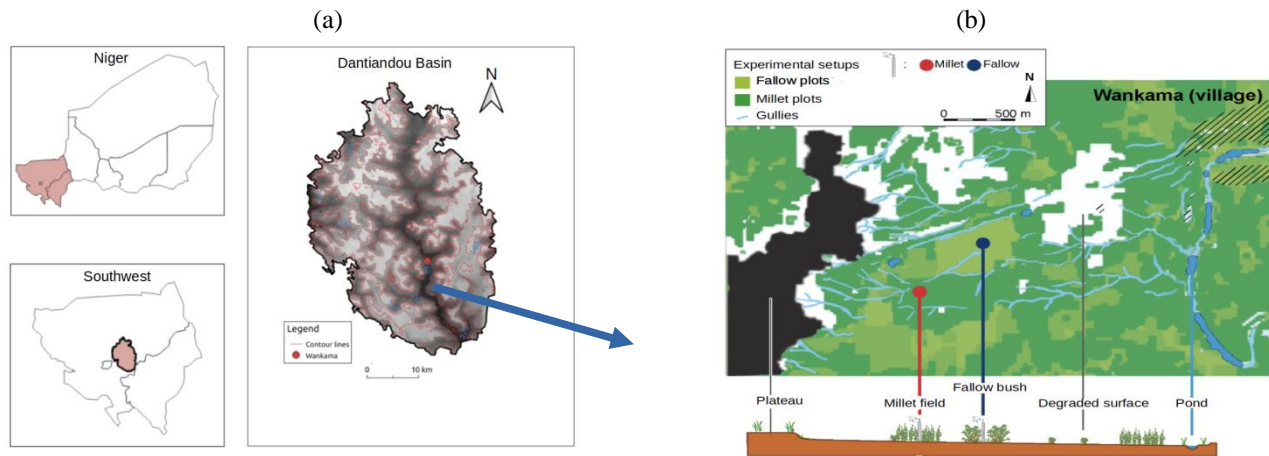


Figure 1. Location of the study area. (a) Location of the Dantiandou Basin in southwestern Niger, including Wankama site, (b) detailed map of the Wankama catchment showing land use, experimental setups and toposequence from the plateau to the pond, including intermediate units.

Two meteorological forcing datasets were used, corresponding to each site. Each site is equipped with an eddy-covariance tower measuring rainfall, air temperature, humidity, atmospheric pressure, wind speed, and shortwave and longwave radiation (Cappelaere et al., 2009; Ramier et al., 2009; Velluet, 2014). Forcing data collected on each site were used to force the model. Figure 2 illustrates the main meteorological variables for the 2006–2011 period at the millet site.

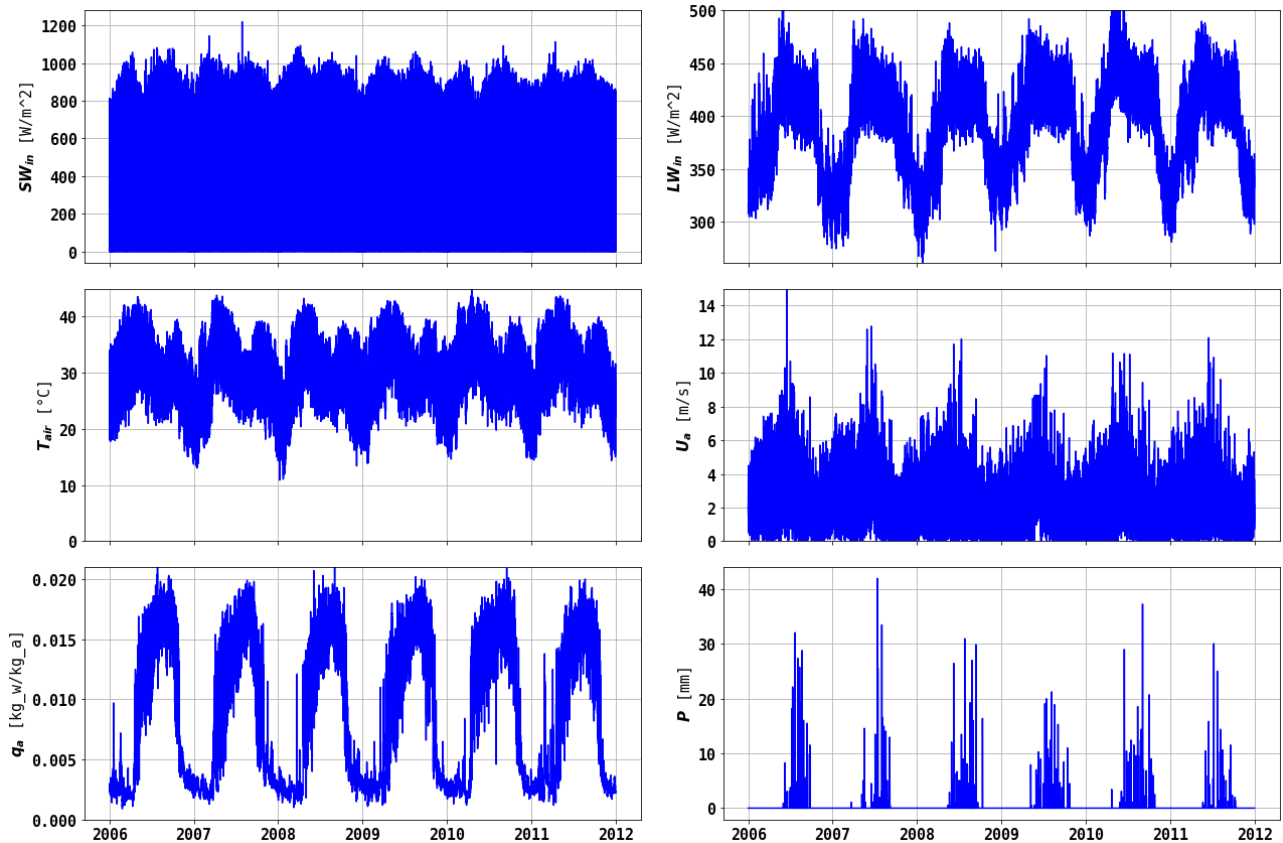


Figure 2 . Model forcing. From the top panel to the bottom: SWin : incoming short waves, LWin : incoming long waves, Tair : air temperature, Ua: wind speed, qa: specific humidity, P : daily precipitation

2.2 Methodology

2.2.1 Description of Par Flow-CLM model

ParFlow-CLM (PF-CLM) is an integrated surface-subsurface coupled hydrological model designed to simulate hydrological processes in the critical zone, integrating both surface and subsurface water flow in three dimensions (Ashby & Falgout, 1996; Jones & Woodward, 2001; Kollet & Maxwell, 2005; Maxwell, 2013). The ParFlow model solves the three-dimensional Richards equation for variably saturated flow using a cell-centered finite difference approach. The model also incorporates a terrain-following grid that accounts for topographic effects and uses a kinematic wave equation to handle overland flow, linking surface and subsurface processes seamlessly (Maxwell, 2013; Kollet & Maxwell, 2006). ParFlow is coupled with the Community Land Model (CLM), which calculates the land-water-energy exchanges, including evapotranspiration which acts as a sink in the Richards equation, according to the root distribution (Dai et al., 2003; Maxwell & Miller, 2005). CLM also handles various surface characteristics such as vegetation, albedo and temperature, influencing surface energy and water fluxes (Dai et al., 2003). This coupling allows the model to represent complex interactions between groundwater and surface water, including the generation of runoff through Hortonian or saturation excess mechanisms (Kollet & Maxwell, 2006; Dunne, 1983; Horton, 1933). ParFlow-CLM's ability to simulate detailed hydrological processes without prior specification makes it particularly suitable for studies in regions like the Sahel.

PF-CLM computes the surface radiative balance using a two-source radiative transfer scheme (soil and canopy) forced by incoming shortwave (SWin) and longwave (Lwin) radiation. When available, the scheme distinguishes between direct and diffuse shortwave components in both the visible and near-infrared bands. This radiative module links soil and canopy temperatures with air temperature based on their optical properties: soil albedo (a function of soil color and moisture), emissivity, and canopy reflectance, transmittance, and emissivity, all parameterized by the Leaf Area Index (LAI).

Soil albedo for direct radiation is computed following Idso et al. (1975):

$$\text{albsod} = \min(\text{albsat} + \text{inc}, \text{albdry}) \quad (1)$$

where albsat and albdry are two parameters depending on the soil color, defining the limits for saturated and dry soil, respectively.

The correction factor inc, which accounts for the influence of volumetric soil water content ($H_2O_{\text{soil,vol}}$), is given by:

$$\text{inc} = \max(a - b \cdot H_2O_{\text{soil,vol}}, 0) \quad (2)$$

The original coefficients of these equations were calibrated by Idso et al. (1975) for arid soils in Arizona. In this study, an iterative calibration was performed to adapt parameters (albsat, albdry, a, b) for both millet and fallow plots, ensuring a better representation of the observed albedo dynamics over Sahelian soils.

The model version used in this study is available at <https://github.com/ige-parflow/parflow-master/releases/tag/v1.0-sahel-min> (last accessed: 18 April 2025).

2.2.2 Model setup

The model domain represents a vertical soil column discretized into five horizons (Figure 3) following the conceptual framework proposed by Velluet (2014). The column is vertically discretized into five soil layers (H1 to H5) corresponding to different horizons characterized by distinct hydraulic properties. The upper layer (H1) interacts with the land surface processes simulated by CLM, including vegetation, infiltration, and evaporation, while the deeper layers (H2–H5) represent subsurface water storage and percolation.

H1 is a 1 cm crusted surface characterized by specific hydrodynamic properties that limit infiltration. The underlying layers correspond to: H2 (1–20 cm), H3 (20–70 cm), H4 (70–120 cm), and H5 (120–3000 cm). The number of grid cells, their respective thicknesses, and the initial soil water contents for millet and fallow plots are summarized in Table 1.

This discretization accounts for (i) soil density heterogeneity, (ii) the crusted surface typical of Sahelian fallows, and (iii) correspondence between observation depths and modeled horizons, facilitating comparison with measured soil moisture profiles.

Table 1. Number of grid cells and initial conditions per soil horizon.

Horizon	H1	H2	H3	H4	H5
Number of grid cells	5	6	6	6	7
Cell thickness (cm)	0.2	3.1	8.3	8.3	40
Initial water content for millet plot (m ³ /m ³)	0.028	0.064	0.13	0.09	0.16
Initial water content for fallow plot (m ³ /m ³)	0.196	0.160	0.153	0.110	0.140

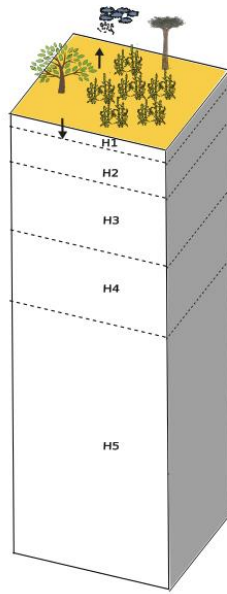


Figure 3. Conceptual representation of the soil column used in simulations.

2.2.3 Model parameters setup and calibration strategy

Initial soil hydraulic parameters were derived from Velluet (2014). These parameters served as the baseline for the ParFlow-CLM simulations before calibration. Calibration process focused on key hydrodynamic parameters : saturated hydraulic conductivity (K_s), Van Genuchten parameters (α and n) which strongly control water balance partitioning (Velluet, 2014; Braud, 1998; Demarty et al., 2004).

The procedure was carried out in two main steps (i) adjust surface parameters controlling rainfall partitioning between infiltration and runoff, and (ii) optimize subsurface parameters governing vertical redistribution and root-zone water availability.

Step 1 – Surface partitioning between infiltration and runoff

400 simulations are performed for each land cover (millet and fallow) over the six years of available meteorological forcing. The parameters K_s , α , and n for the surface crust (H1) are sampled using a Latin Hypercube Sampling method (McKay et al., 1979) (Table 2). Then the 20 best-performing parameter sets were selected based on two criteria:

(i) the Kling–Gupta Efficiency (KGE) (Kling et al., 2012) for evapotranspiration during rainy season onset (April–July), and

(ii) simulated runoff coefficients within observed ranges: 5–15% for the millet plot and 7–21% for the fallow plot (Bouzou et al., 2020).

The final optimal parameter set was first defined as the arithmetic mean of the 20 retained parameter sets. Minor manual adjustments were applied within physically plausible ranges, following a limited trial-and-error procedure. to ensure the consistency of simulated fluxes.

Step 2 - Water redistribution in the root zone

Using the optimized surface parameters from Step 1, a new set of 400 simulations is conducted to calibrate horizons H2 and H3. The same sampling and calibration approach was applied, but focusing on evapotranspiration performance during end of rainy season (November–December). The 20 best parameter sets are again averaged and slightly adjusted to find the final optimal values for these layers, ensuring adequate water redistribution and root uptake in the root zone.

Step 3 - Optimization of surface radiative parameters

Original radiative parameters of Idso et al. (1975), calibrated for arid zones in Arizona, cannot reproduce the observed albedo dynamics over Sahelian soils. An iterative calibration is therefore conducted to adjust the parameters of equations. (1) and (2) for both millet and fallow plots. Vegetation parameters were prescribed according to AMMA-CATCH field observations and previous modeling work (Velluet 2014).

Table 2. Parameter ranges explored during calibration for both sites.

Parameter	Description	Unit	Range
K_{s1}	Hydraulic conductivity / H1	$m \cdot h^{-1}$	$[6.12 \times 10^{-5} ; 7.2 \times 10^{-3}]^{i,j,k}$
h_{g1}	Matric potential / H1	m	$[-2.4 ; -0.31]^{i,j}$
n_1	VG parameter n / H1	-	$[2.35 ; 3.53]^{i,j}$
K_{s2}	Hydraulic conductivity / H2	$m \cdot h^{-1}$	$[1.44 \times 10^{-2} ; 2.52 \times 10^{-1}]^{i,n}$
h_{g2}	Matric potential / H2	m	$[-0.6 ; -0.06]^{i,j,l,m}$
n_2	VG parameter n / H2	-	$[2.55 ; 4.2]^{i,j,l,m}$

i Braud et al. (1997), j Simunek et al. (1998), k Vandervaere et al. (1997), l Manyame et al. (2007), m Rockström et al. (1998), n Gaze et al. (1997)

2.2.4 Model evaluation

Model performance was evaluated at half-hourly and daily time steps using standard statistical criteria: the root mean square error (RMSE), bias, Pearson correlation (r), Nash–Sutcliffe efficiency (NSE), and Kling–Gupta efficiency (KGE). These metrics were computed for surface energy fluxes and soil moisture at different depths over the evaluation period (2006–2011), using the following formulas, respectively:

• Root Mean Square Error (RMSE)

$$RMSE = \sqrt{\frac{1}{N} * \sum (P_i - O_i)^2} \quad (3)$$

where N = total number of observations

P_i = simulated value at time step i

O_i = observed value at time step i

RMSE quantifies the average magnitude of the model error; lower values indicate better performance.

• Bias

$$Bias = \frac{1}{N} * \sum (P_i - O_i) \quad (4)$$

with N = total number of observations

P_i = simulated value at time step i

O_i = observed value at time step i

Bias measures the mean tendency of simulated values to be larger (positive bias) or smaller (negative bias) than observed values.

• **Pearson correlation coefficient (r)**

$$r = \frac{[\sum((O_i - \bar{Y}_O)(P_i - \bar{Y}_P))]}{\sqrt{[\sum(O_i - \bar{Y}_O)^2 * \sum(P_i - \bar{Y}_P)^2]}} \quad (5)$$

where \bar{Y}_O = mean of observed values

\bar{Y}_P = mean of simulated values

P_i, O_i = simulated and observed values at time step i

r quantifies the strength and direction of the linear relationship between observed and simulated values ($r \in [-1, 1]$).

• **Nash–Sutcliffe Efficiency (NSE)**

$$NSE = 1 - \frac{\sum(O_i - P_i)^2}{\sum(O_i - \bar{Y}_O)^2} \quad (6)$$

where O_i = observed value at time step i

P_i = simulated value at time step i

\bar{Y}_O = mean of observed values

NSE indicates model predictive skill relative to the mean of observations. Values close to 1 indicate high model performance, while values below 0 suggest poor performance.

• **Kling–Gupta Efficiency (KGE)**

$$KGE = 1 - \sqrt{(r - 1)^2 + (\alpha - 1)^2 + (\beta - 1)^2} \quad (7)$$

where r = Pearson correlation coefficient

$\alpha = \sigma_P / \sigma_O$ (ratio of simulated to observed standard deviations)

$\beta = \mu_P / \mu_O$ (ratio of simulated to observed means)

σ_P, σ_O = standard deviations of simulated and observed values

μ_P, μ_O = means of simulated and observed values

KGE decomposes performance into correlation, variability, and bias components for comprehensive model assessment.

3 Results

3.1 Model calibration

For the millet field, calibration mainly affected the hydraulic properties of the surface crust (H1). The saturated hydraulic conductivity (K_s) was adjusted to $8.5 \times 10^{-4} \text{ m} \cdot \text{h}^{-1}$, slightly below the initial estimate used by Velluet et al. (2014), in order to reproduce the observed infiltration–runoff partitioning. Despite this moderate K_s value, infiltration limitation remains primarily governed by the ratio e/K_s , where e is the crust thickness (1 cm in the model). Because the actual crust observed in the field is only a few millimeters thick, the chosen value ensures a realistic representation of the infiltration process.

The shape parameter (n) decreased from 1.75 to 1.4, increasing the water-holding capacity of the surface layer, while the air-entry pressure ($|h_g|$) was set to 2.08 m, indicating a smoother retention curve and enhanced soil moisture retention near the surface. In the subsurface horizons (H2–H5), the parameters were kept relatively homogeneous ($K_s \approx 0.18 \text{ m} \cdot \text{h}^{-1}$; $n \approx 2.0$ – 2.1 ; $|h_g| = 0.2$ – 0.3 m), reflecting a sandy profile with moderate drainage capacity and limited

vertical contrasts. These adjustments reduced the initial overestimation of runoff and improved the seasonal dynamics of soil moisture and evapotranspiration.

For the fallow plot, calibration resulted in a lower surface hydraulic conductivity ($K_s = 4.81 \times 10^{-4} \text{ m}\cdot\text{h}^{-1}$) compared to millet, consistent with the presence of a denser and more stable crust limiting infiltration. Below the surface, the K_s values progressively increased to $\approx 0.25 \text{ m}\cdot\text{h}^{-1}$ in the deeper horizons, indicating a profile more favorable to percolation. The air-entry pressure ($|h_g|$) ranged between 0.2 and 0.66 m, while the shape parameter (n) varied from 1.5 in H1 to 2.34 in H3, reflecting greater heterogeneity in soil structure and a stronger capillary retention capacity than in millet soils. This configuration reproduces well the observed persistence of moisture in the upper layers of fallow soils after rainfall events, as well as their slower drying rate during the dry season.

Table 3. Calibrated soil hydraulic parameters for each horizon. Values in bold indicate parameters adjusted during calibration.

Land cover	Horizon	$K_s [\text{m}\cdot\text{h}^{-1}]$	$ h_g [\text{m}]$	$n [-]$	$\theta_r [\text{m}^3\cdot\text{m}^{-3}]$	$\theta_s [\text{m}^3\cdot\text{m}^{-3}]$
Millet	H1	8.5×10^{-4}	2.08	1.4	0.028	0.9
	H2	0.18	0.3	2.1	0.064	
	H3	0.18	0.3	2.0	0.14	
	H4	0.18	0.2	2.0	0.13	
	H5	0.18	0.2	2.0	0.16	
Fallow	H1	4.81×10^{-4}	2.0	1.5	0.028	0.9
	H2	0.252	0.66	1.7	0.033	
	H3	0.18	0.54	2.34	0.087	
	H4	0.252	0.3	2.0	0.075	
	H5	0.252	0.2	2.3	0.1	

3.2 Surface albedo calibration and evaluation

Surface albedo calibration improved the simulation of radiative exchanges for both land covers. Table 4 summarizes the visible and infrared albedo parameters before and after calibration. On the **millet plot** (Figure 5.a), the simulated albedo using the default parameters systematically underestimated the seasonal variations and amplitude observed in the field. After calibration, the simulated curve closely follows the observed dynamics, particularly the sharp decreases following major rainfall events and the progressive increases during the dry-down periods. The calibrated simulation reproduces both the annual cycle and interannual variability. For the **fallow plot** (Figure 5.b), the calibrated simulation also shows improved agreement with observations, capturing the higher baseline albedo and the dampened seasonal amplitude compared to millet. The increase in the dry albedo parameter reflects the lighter soil color and sparse vegetation cover typical of the fallow. The model reproduces the rapid wetting responses during the rainy season and the gradual recovery of surface brightness in the dry season.

Table 4. Comparison of surface radiative parameters (albedo) before and after calibration.

	Millet		Fallow	
Parameters	Visible	Infrared	Visible	Infrared

	Before	After	Before	After	Before	After	Before	After
albdry	0.34	0.326	0.68	0.652	0.24	0.345	0.48	0.690
albsat	0.20	0.135	0.40	0.270	0.12	0.126	0.24	0.252
a	0.11	0.17	0.11	0.17	0.11	0.17	0.11	0.17
b	0.40	0.60	0.40	0.60	0.40	0.60	0.40	0.60

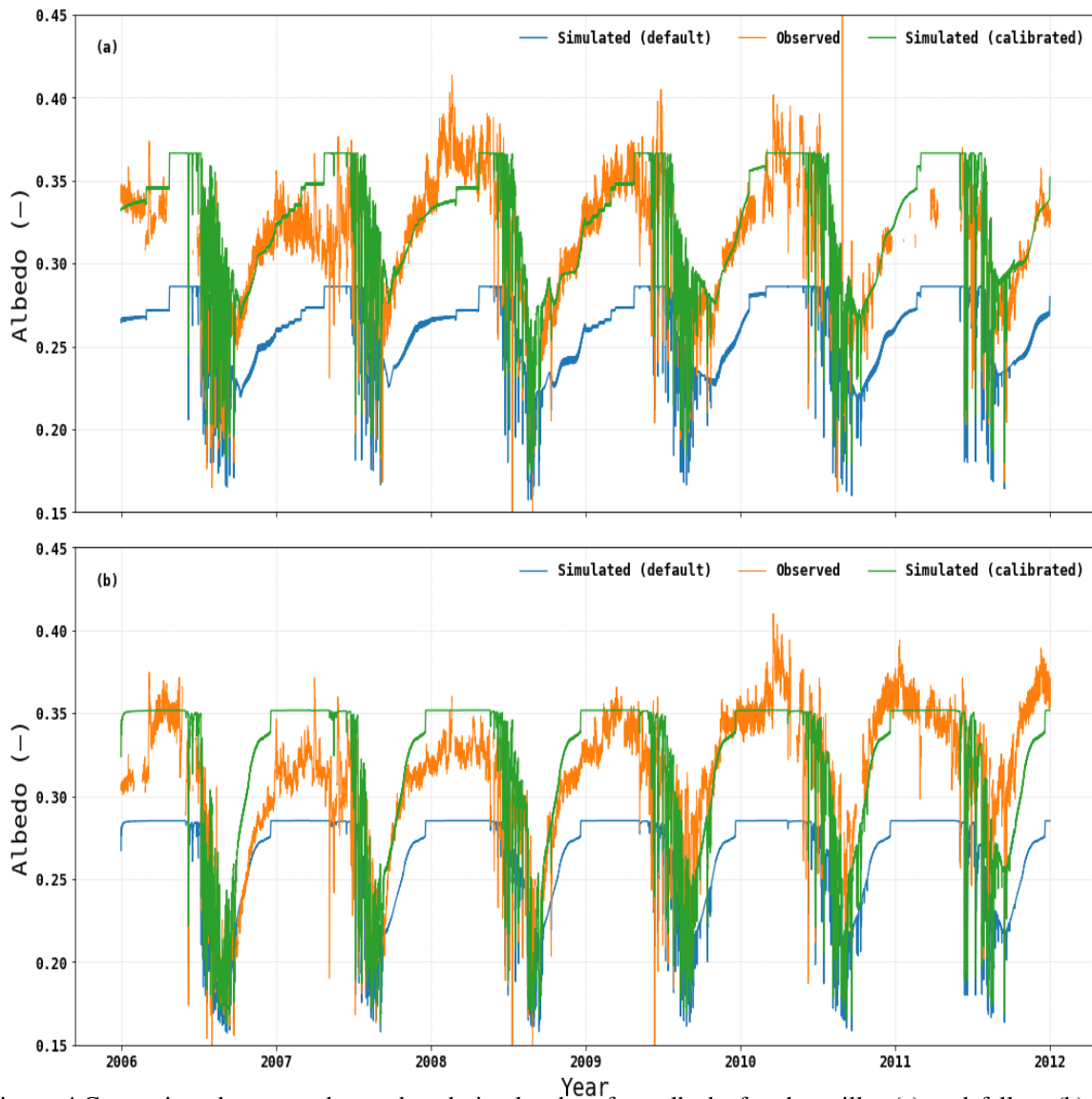


Figure 4. Comparison between observed and simulated surface albedo for the millet (a) and fallow (b) plots at Wankama from 2006 to 2011. “Simulated (default)” refers to simulations using the initial radiative parameters, while “Simulated (calibrated)” corresponds to the optimized parameters after calibration

3.3 Evaluation of simulated energy fluxes

The comparison between observed and simulated radiative fluxes over the millet (left column) and fallow (right column) plots (Figure 4) shows that the model reproduces net radiation reasonably well at both sites. The dry-season

positive bias in R_n , particularly over the fallow, results from an underestimation of outgoing longwave radiation (LWout), partly compensated by a slight overestimation of reflected shortwave radiation (SWout). Despite these discrepancies, model performance for the radiative components remains satisfactory. Over the millet plot, SWout and LWout show RMSE values of 7.7 W m^{-2} with strong correlations (0.84 and 0.94), while errors increase over the fallow plot (RMSE of 10.5 W m^{-2} for SWout and 13.9 W m^{-2} for LWout), reflecting the enhanced radiative variability of bare-soil conditions.

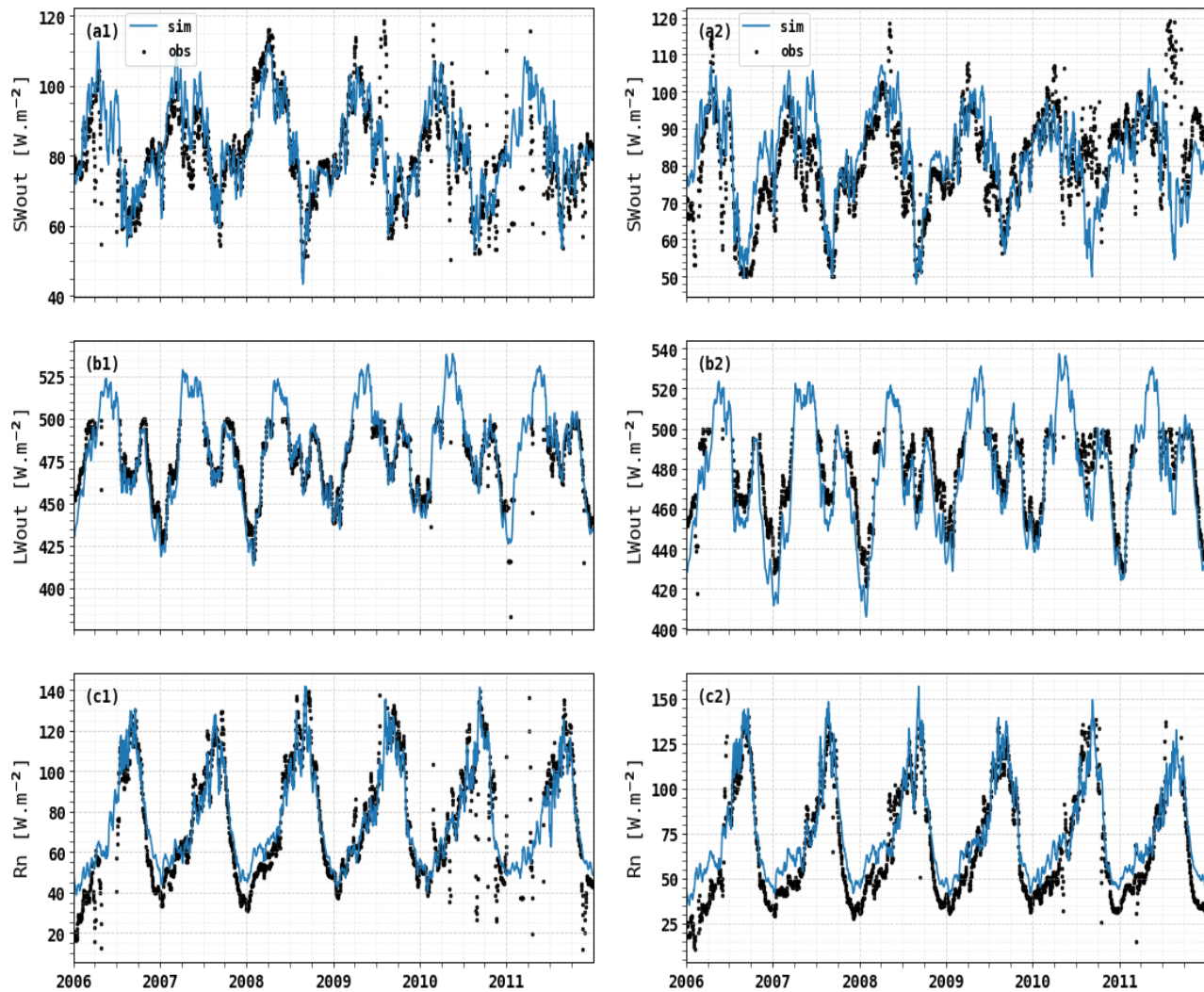


Figure 4 Comparison of observed and simulated surface radiation fluxes over millet (left) and fallow (right) plots from 2006 to 2011. Panels show (a) outgoing shortwave radiation (SWout), (b) outgoing longwave radiation (LWout), and (c) net radiation (R_n).

Table 5. Evaluation of simulated energy fluxes (RMSE, KGE, Bias, NSE, Correlation).

Land cover	Variable	RMSE	KGE	Bias	NSE	Corr.
Millet	SW _{out}	7.7	0.80	2.88	0.66	0.84
	LW _{out}	7.7	0.84	-1.80	0.84	0.94
	Rn	12.0	0.74	0.45	0.83	0.92
	Albedo	0.02	0.78	0.01	0.63	0.83
Fallow	SW _{out}	10.5	0.65	2.57	0.30	0.66
	LW _{out}	13.91	0.88	-11.91	0.50	0.94
	Rn	12.26	0.75	6.42	0.82	0.93
	Albedo	0.03	0.80	0.01	0.56	0.81

3.4 water balance evaluation

At the beginning of the rainy season, nearly all rainfall is lost through evaporation at both sites, with peak daily rates reaching about 4 mm d⁻¹ for the fallow and 2.86 mm d⁻¹ for the millet plot (Figure 5a–b). Transpiration at both sites follows the seasonal rise of LAI, starting around mid-July and increasing toward the peak of the growing season.

Figure 5c–d present the simulated annual water budgets for both sites. Evapotranspiration is the dominant component, representing on average 82 % of annual rainfall over the millet plot and 88 % over the fallow. The higher value for the fallow mainly reflects its greater evaporation (57 % vs. 47 %), driven by limited vegetation cover and increased exposure of bare soil. In contrast, transpiration contributes similarly at both sites (≈ 31 –34 %), indicating comparable plant water use efficiency despite lower biomass in the fallow.

Runoff accounts for 16 % of rainfall in the millet plot and 13 % in the fallow, the latter showing slightly reduced surface flow due to weaker crust formation and lower compaction. Deep drainage is negligible or slightly negative at both sites (≈ -1 % of P), indicating minimal percolation and occasional upward fluxes during dry periods. Changes in soil water storage remain modest (± 4 %), with small gains in wetter years and deficits in drier ones, confirming that soil moisture variability is largely restricted to the upper soil layers and tightly controlled by evaporation–transpiration dynamics.

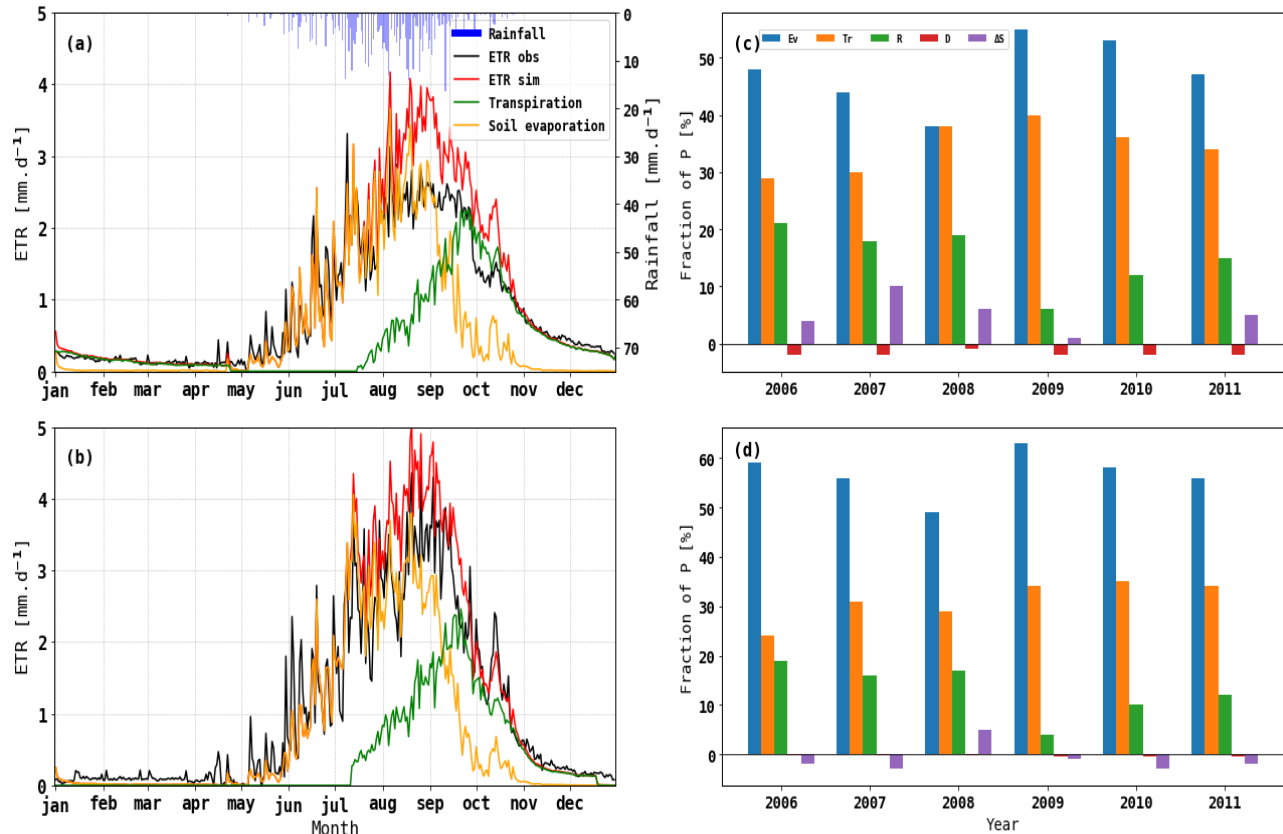


Figure 5 Seasonal observed and simulated actual evapotranspiration (ETR) for millet (a) and fallow (b) plots, with simulated transpiration (green), soil evaporation (orange), and daily rainfall (blue bars). Panels (c) and (d) show the corresponding annual partitioning of rainfall into Ev, Tr, R, D and ΔS .

3.5 Soil moisture profiles

Figures 6 and 7 show comparison between observed and simulated soil moisture dynamics for different depths under both millet and fallow plots. PF-CLM successfully reproduces the temporal variability and vertical gradients and captures the main seasonal wetting and drying cycles in response to rainfall events, especially in the upper layers.

For the millet plot (Figure 6), soil moisture at 10 cm and 50 cm is well reproduced, with Kling-Gupta efficiencies (KGE) of 0.81 and 0.69, respectively. The model correctly simulates the infiltration pulses following major rainfall events and the subsequent drying during inter-storm periods. At deeper depths (≥ 100 cm), the temporal dynamics are smoother, reflecting the slower percolation of water and the reduced influence of rainfall variability. The model maintains reasonable performance down to 250 cm (KGE ≈ 0.25 ; NSE ≈ 0.21), although a slight underestimation of moisture persistence is observed at 150–200 cm.

For the fallow plot (Figure 7), simulated moisture profiles also show good agreement in the upper 100 cm (KGE = 0.65–0.78; NSE = 0.42–0.62), consistent with the lower infiltration rates and higher surface retention associated with persistent shrubs and crusted surface. However, at deeper horizons (> 150 cm), model performance declines significantly (negative NSE and KGE values), suggesting an overestimation of drainage or insufficient representation of subsoil water retention processes.

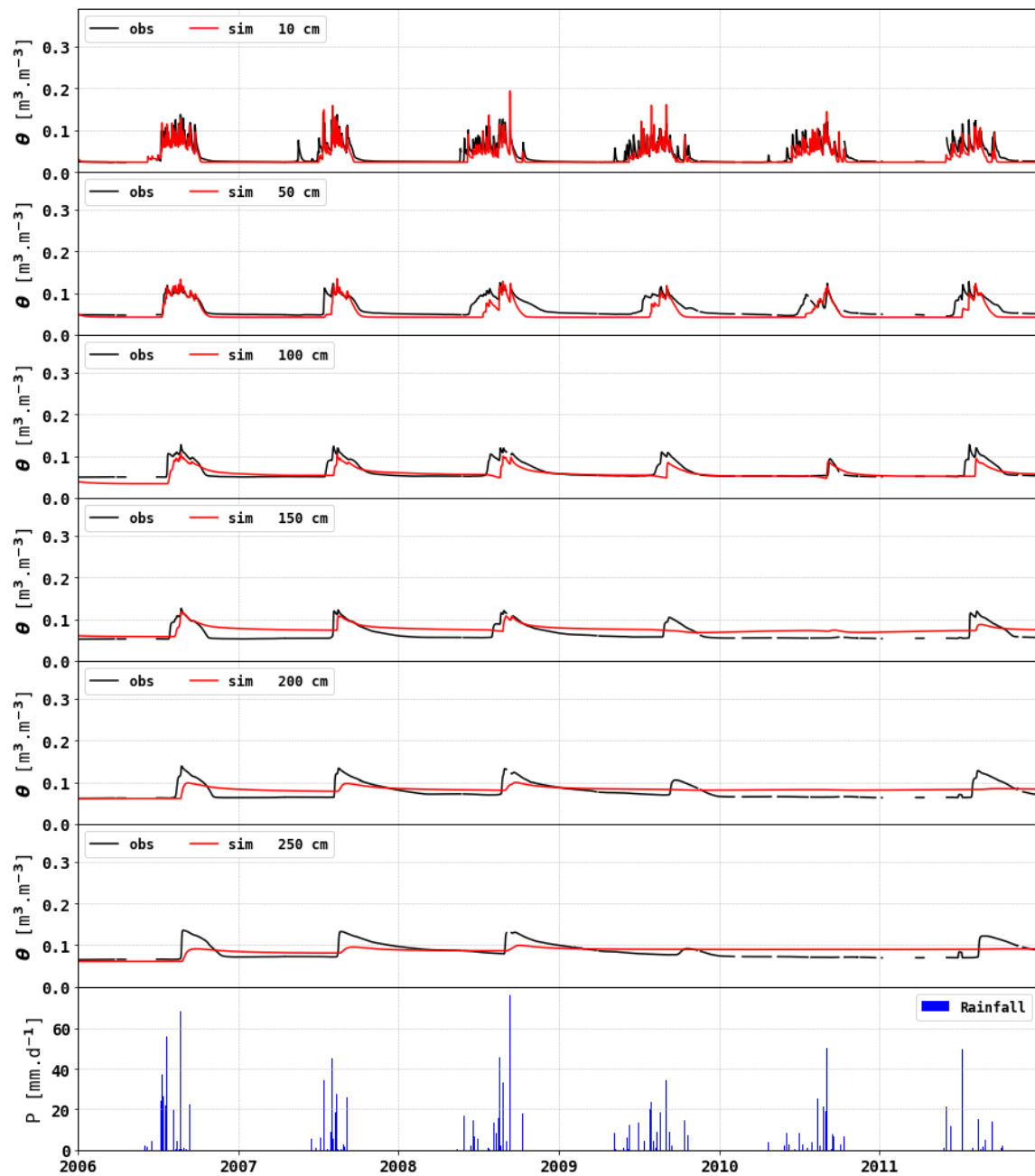


Figure 6. Simulated (red) and observed (black) soil water content at different depths for the millet plot, together with daily rainfall (blue).

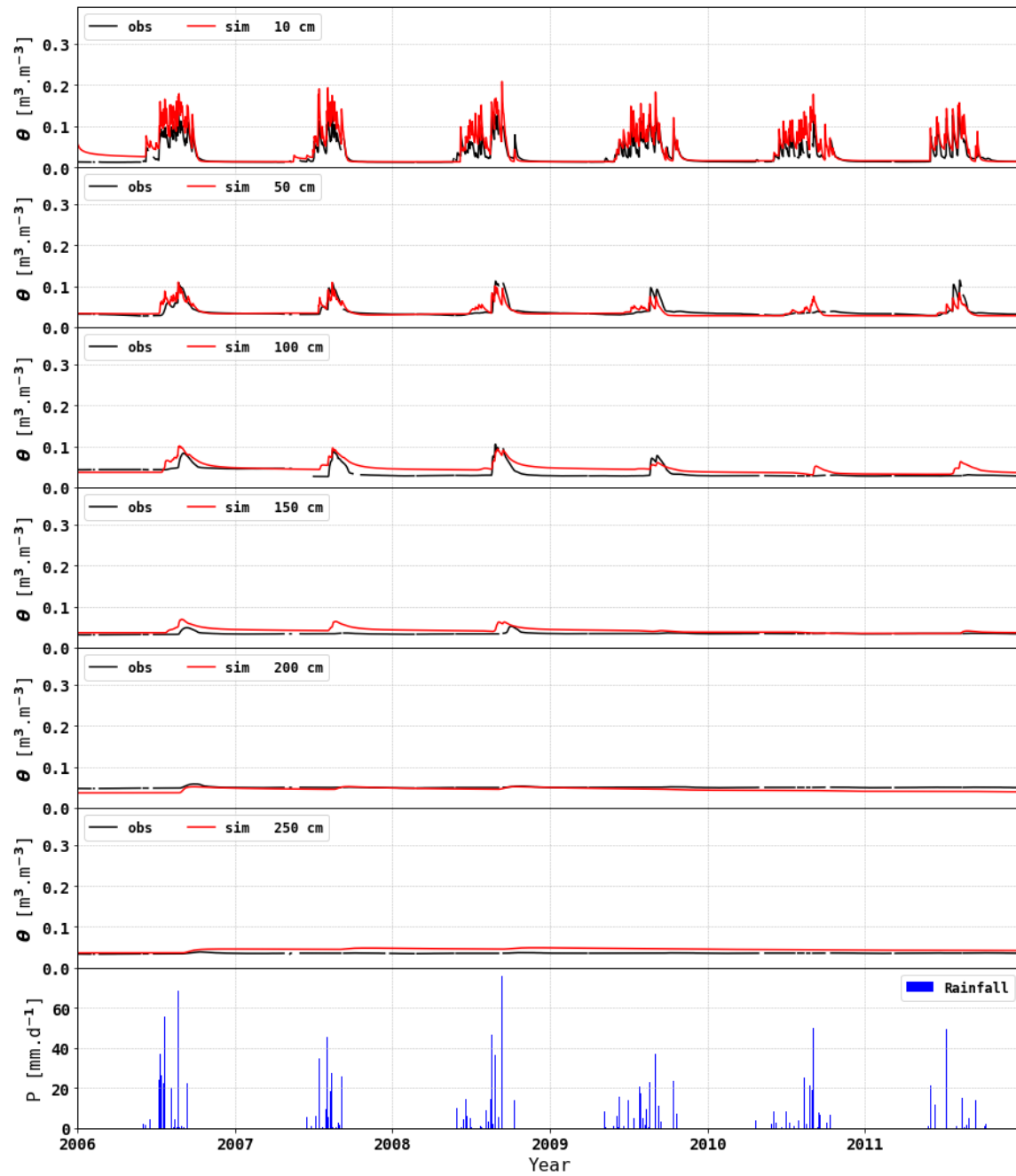


Figure 7. Simulated (red) and observed (black) soil water content at different depths for the fallow plot, together with daily rainfall (blue).

Table 6. Evaluation of simulated soil moisture profiles (RMSE, KGE, Bias, NSE, Correlation).

Land cover	Depth (cm)	RMSE	KGE	Bias	NSE	Corr.
	10	0.01	0.81	0.01	0.71	0.88

Millet	50	0.02	0.69	-0.01	0.37	0.83
	100	0.01	0.55	0.0	0.42	0.68
	150	0.02	0.31	0.01	-0.02	0.61
	200	0.01	0.23	0.0	0.21	0.52
	250	0.02	0.25	0.0	0.21	0.46
Fallow	10	0.02	0.65	0.01	0.42	0.92
	50	0.01	0.78	0.0	0.62	0.80
	100	0.01	0.56	0.01	-0.07	0.74
	150	0.01	-0.11	0.01	-10.64	0.53
	200	0.01	-1.48	0.01	-21.13	0.49
	250	0.01	-1.44	0.01	-136.89	0.55

4 Discussion

The ParFlow–CLM simulations reproduce the main seasonal patterns of energy and water exchanges observed at the Wankama millet and fallow sites, showing model's ability to capture the strong coupling between monsoonal rainfall and soil moisture dynamics that characterize the Sahel. The model also represents well energy budget components while some biases remain in the dry season net radiation due to underestimation of longwave emission and overestimation of soil albedo during bare-soil periods. Similar deviations were also reported by Velluet et al. (2014) with SiSPAT, highlighting the challenges of representing soil optical properties under strong seasonal contrast and rapid post-rain surface changes (Timouk et al., 2009).

4.1 Surface fluxes and energy closure

The improved simulation of net radiation and the partitioning between latent and sensible heat fluxes result from the iterative calibration of radiative parameters (albdry, albsat, a, b). The resulting seasonal albedo variations now agree with field measurements, eliminating the systematic dry-season bias initially found using the Idso et al. (1975) parameterization. The performance metrics obtained indicate that ParFlow–CLM reproduces the diurnal and seasonal energy balance with an accuracy comparable to or better than SiSPAT. The remaining discrepancies in soil heat flux (negative KGE at both sites) reflect the known difficulty of reproducing the amplitude and phase of ground heat storage in semi-arid environments, where rapid drying limits conduction at the surface (Braud et al., 1995; Velluet et al., 2014).

4.2 Soil moisture profiles

Vertical soil moisture profiles simulated by ParFlow–CLM are in close agreement with observations down to 50 cm (KGE between 0.7 and 0.8), confirming the model's realistic representation of infiltration and surface evaporation. However, performance decreases with depth, particularly below 150 cm where NSE becomes negative for the fallow site. These results are consistent with previous findings by Velluet et al. (2014), who showed that the dynamics at these depths are strongly influenced by the sparse root systems and low hydraulic connectivity typical of Sahelian soils. The smoother and weaker deep fluctuations in ParFlow–CLM may also reflect differences in the vertical distribution of soil hydraulic conductivity and the explicit representation of capillary rise, which SiSPAT does not account for. Despite these limitations, the model reproduces the observed contrast between the millet (higher near-surface variability linked to cultivation and soil disturbance) and the fallow (greater stability due to crust formation and reduced infiltration).

Several structural and process-related limitations can explain the strong decrease in model performance in the deeper soil layers under fallow conditions below 150 cm. First, the sparse and shallow root systems typical of Sahelian fallow vegetation reduce the sensitivity of deep soil moisture to transpiration, making observed signals weak and difficult to reproduce numerically. Second, uncertainties in the vertical distribution of soil hydraulic properties, particularly hydraulic conductivity in deeper layers, may affect the representation of slow percolation and capillary exchanges. In ParFlow–CLM, the explicit simulation of vertical pressure gradients and capillary rise may lead to smoother deep soil moisture dynamics than observed, especially in soils characterized by low hydraulic connectivity and strong textural contrasts. These limitations highlight the difficulty of constraining deep soil processes in semi-arid environments and partly explain the reduced performance metrics at depth.

4.3 Annual water balance and comparison with SiSPAT

At the annual scale, both models predict evapotranspiration as the dominant term of the water balance, accounting for approximately 75–88% of annual rainfall, in agreement with field estimates at Wankama (Velluet et al., 2014). To facilitate the interpretation of the differences in simulated water balance components, Table 7 summarizes the main differences in process representation between ParFlow–CLM and SiSPAT.

Table 7. Comparison of the main characteristics of ParFlow–CLM and SiSPAT models in a 1D configuration.

Aspect	ParFlow–CLM	SiSPAT
Model type	Fully integrated, physically based	Physically based SVAT model (1D)
Surface–subsurface coupling	Explicit coupling with pressure continuity at the surface–subsurface interface	Implicit coupling within a 1D soil–vegetation–atmosphere framework
Lateral flow	Possible (disabled in 1D setup)	Not represented
Soil moisture dynamics	Fully resolved Richards equation	Mechanistic vertical transfers solving coupled heat and mass transfer equations (including vapor phase)
Capillary rise	Explicitly represented through vertical pressure gradients	Vertical redistribution including capillarity within the soil profile; depends on prescribed bottom boundary condition
Root water uptake	Distributed within the soil profile	Parameterized root water uptake
Runoff generation	Sensitive to surface hydraulic properties and roughness (overland flow formulation)	Limited representation through surface boundary conditions
Deep drainage	Small, can be negative (upward redistribution fluxes)	Negligible or zero in the present 1D configuration
Energy balance	Fully coupled with CLM	Explicit surface energy balance
Strengths	Process consistency; explicit surface–subsurface coupling	Robust representation of surface fluxes and soil–atmosphere exchanges
Limitations	Computational cost; uncertainty in deep soil processes	No lateral flow; deep processes constrained by boundary conditions

ParFlow–CLM yields higher runoff than SiSPAT but similar or slightly lower deep drainage, which remains negligible or negative at both sites. For the millet plot, runoff represents about 72 mm yr^{-1} , while deep drainage is extremely small and slightly negative ($\approx -8 \text{ mm yr}^{-1}$), indicating a weak upward flux towards the root zone rather than effective percolation. This behaviour reflects the combined effects of high evaporative demand, shallow active soil layers, and limited hydraulic conductivity at depth. The fallow plot shows similar patterns, with slightly lower runoff ($\approx 61 \text{ mm yr}^{-1}$) and negligible drainage (≈ -1 to -3 mm yr^{-1}). Overall, ParFlow–CLM suggests that under present climatic conditions, both land covers favour very limited groundwater recharge, with most infiltrated water returning to the atmosphere through evaporation and transpiration. These differences stem from the explicit coupling of surface and subsurface flow in ParFlow, which enhances the hydrological response to rainfall events and produces small but systematic redistribution fluxes within the deep soil, although effective downward percolation remains negligible under current conditions. The larger runoff in ParFlow is consistent with the high sensitivity of infiltration to soil crusting and roughness observed in the field (Peugeot et al., 1997; Bouzou et al., 2020). In contrast, SiSPAT, which

neglects lateral exchanges, confines most rainfall losses to evaporation, resulting in lower drainage. The emergence of small but systematic drainage fluxes in ParFlow–CLM supports the possibility of episodic deep percolation and local recharge events, as suggested by Favreau et al. (2009) and Massuel et al. (2011).

For the fallow site, ParFlow–CLM and SiSPAT predict comparable evapotranspiration but diverge in subsurface fluxes. ParFlow simulates a mean annual evaporation of 262 mm and negative drainage values, whereas SiSPAT predicts 279 mm of evaporation with no drainage. These contrasts confirm that ParFlow–CLM better represents the slow redistribution of soil water between seasons, while SiSPAT tends to close the balance at the soil surface. The small interannual variations in storage (ΔS between -10 and $+25$ mm.yr⁻¹) also indicate that the deeper soil layers contribute to regulating surface fluxes across years—an aspect that the integrated ParFlow–CLM framework is specifically designed to capture.

4.4 Model implications and outlook

Overall, ParFlow–CLM reproduces the observed hydroclimatic functioning of Sahelian ecosystems while providing a more physically based description of the soil–atmosphere–aquifer continuum than SiSPAT. The 1D configuration allows isolating key vertical processes—soil evaporation, root uptake, and percolation—before extending the model to 2D hillslopes, where lateral redistribution, runoff–runoff interactions, and microtopographic effects become dominant (Descroix et al., 2018). Beyond validation, this comparison demonstrates that ParFlow–CLM can serve as a process-based tool for exploring the long-term impacts of land degradation and sustainable land management on water resources in the Sahel. Future work will exploit the integrated modeling framework to quantify how surface condition changes (e.g., sustainable land management practices) modify infiltration–runoff partitioning and groundwater recharge under variable climate forcing.

5 CONCLUSION

This study evaluated the ability of the integrated hydrological model ParFlow-CLM to reproduce the seasonal and interannual dynamics of water and energy exchanges in the cultivated Sahel, using long-term observations from the Wankama experimental **site** in Niger. The 1D simulations conducted over millet and fallow plots successfully captured the main features of the local hydroclimatic cycle—strongly seasonal rainfall, rapid surface drying, and vegetation-controlled evapotranspiration—confirming the model’s robustness under semi-arid conditions.

Comparison with the SiSPAT results of Velluet et al. (2014) showed that ParFlow-CLM reproduces comparable magnitudes of evapotranspiration (≈ 75 – 85 % of annual rainfall) and captures the distinct hydrological behaviors of the two covers: higher evaporation over fallow and slightly higher runoff under millet, while deep drainage remains negligible or slightly negative for both land covers. Differences in runoff and drainage primarily arise from ParFlow’s explicit coupling between surface and subsurface flow, which allows limited percolation and storage in deeper soil layers, processes that are not explicitly coupled to surface flow and are constrained by boundary conditions in SiSPAT.

Overall, the findings highlight the capability of ParFlow-CLM to represent the full soil–plant–atmosphere continuum within a physically consistent framework. The results also emphasize the key role of surface optical and hydraulic properties in controlling energy partitioning and infiltration–runoff processes in the Sahel. Future work will extend this 1D framework to 2D hillslope and catchment scales to investigate lateral redistribution, runoff connectivity, and the hydrological impacts of sustainable land management practices on groundwater recharge and surface water generation.

References

1. Ashby, S. F., & Falgout, R. D. (1996). A parallel multigrid preconditioned conjugate gradient algorithm for groundwater flow simulations. *Nuclear science and engineering*, 124(1), 145-159.
2. Bouzou, M. et al. (2020). Long-term impacts of soil crusting and land use on runoff in the Sahel. *Hydrol. Earth Syst. Sci.*, 24, 1339–1354.
3. Bodjrénou, R., Sintondji, L. O., & Comandan, F. (2023). Hydrological modeling with physics-based models in the Ouémé basin: Issues and perspectives for simulation optimization. *Journal of Hydrology: Regional Studies*, 48, 101448. <https://doi.org/10.1016/j.ejrh.2023.101448>

4. Bodjrènou, R., Sintondji, L. O., & Comandan, F. (2025a). Revealing the spatiotemporal precipitation patterns of ECMWF fifth-generation reanalyses since the mid-20th century in West-Africa. *Environmental Advances*, 20, 100636. <https://doi.org/10.1016/j.envadv.2025.100636>
5. Bodjrènou, R., Sintondji, L. O., Sambieni, S. K., Tidjani, N., Koyo, P., Avossè, A., & Comandan, F. (2025b). Analysis of current and future climate variability and drought recurrence in Benin, West Africa. *Journal of Water and Climate Change*, 16(7), 2297–2316. <https://doi.org/10.2166/wcc.2025.842>
6. Braud, I. et al. (1995). SiSPAT: A model for the simulation of water and energy transfer in the soil–plant–atmosphere continuum. *J. Hydrol.*, 166, 213–250.
7. Braud, I., Dantas-Antonino, A. C., Vauclin, M., Thony, J.-L., and Ruelle, P. (1995). SiSPAT: A model for the simulation of water and energy transfers in the soil–plant–atmosphere system. *Journal of Hydrology*, 166(3–4), 213–250.
8. Braud, I., Bessemoulin, P., Monteny, B., Sicot, M., Vandervaere, J., Vauclin, M., 1997. Uni-dimensional modelling of a fallow savannah during the hapex-sahel experiment using the SiSPAT model. *Journal of Hydrology* 188, 912–945.
9. Casenave, A., & Valentin, C. (1992). A runoff capability classification system based on surface features criteria in semi-arid areas of West Africa. *Journal of Hydrology*, 130(1–4), 231–249.
10. Descroix, L., Moussa, I. B., Genthon, P., Sighomnou, D., Mahé, G., Vandervaere, J.-P., ... & Mamadou, I. (2018). Evolution of surface hydrology in the Sahel under increasing land pressure and climate change. *Comptes Rendus Geoscience*, 350(7), 312–323.
11. Diongue, D. M., Rounsard, O., Do, F. C., Stumpp, C., Orange, D., Sow, S., ... & Faye, S. (2022). Evaluation of parameterisation approaches for estimating soil hydraulic parameters with HYDRUS-1D in the groundnut basin of Senegal. *Hydrological Sciences Journal*, 67(15), 2327-2343.
12. Diouf, O. C., Weihermüller, L., Diedhiou, M., Vereecken, H., Faye, S. C., Faye, S., & Sylla, S. N. (2020). Modelling groundwater evapotranspiration in a shallow aquifer in a semi-arid environment. *Journal of Hydrology*, 587, 124967.
13. Favreau, G. et al. (2009). Land clearing, climate variability, and water resources increase in semiarid southwest Niger: A modeling perspective. *Water Resour. Res.*, 45, W00A16.
14. Galle, S. et al. (1999). Water balance of a cultivated Sahelian catchment. *J. Hydrol.*, 216, 244–263.
15. Ibrahim, M., Favreau, G., Scanlon, B. R., Seidel, J. L., Le Coz, M., Demarty, J., & Cappelaere, B. (2014). Long-term increase in diffuse groundwater recharge following expansion of rainfed cultivation in the Sahel, West Africa. *Hydrogeology Journal*, 22(6), 1293-1305.
16. Gaze, S., Simmonds, L., Brouwer, J., Bouma, J., 1997. Measurement of surface redistribution of rainfall and modelling its effect on water balance calculations for a millet field on sandy
17. soil in niger. *Journal of Hydrology* 188, 267–284
18. Idso, S. et al. (1975). Relation between soil albedo and soil water content. *J. Appl. Meteorol.*, 14, 109–113.
19. Kassam, A. H., & Kowal, J. M. (1975). Water use, energy balance and growth of groundnut at Samaru, Northern Nigeria. *Agricultural Meteorology*, 15(1), 33–47.
20. Kollet, S. J., & Maxwell, R. M. (2008). Capturing the influence of groundwater dynamics on land surface processes using an integrated, distributed watershed model. *Water Resources Research*, 44, W02402.
21. Lebel, T., & Ali, A. (2009). Recent trends in the Central and Western Sahel rainfall regime (1990–2007). *Journal of hydrology*, 375(1-2), 52-64.
22. Massuel, S., Cappelaere, B., Favreau, G., Leduc, C., Lebel, T., & Vischel, T. (2011). Integrated surface water–groundwater modelling in the context of increasing water reserves of a regional Sahelian aquifer. *Hydrological Sciences Journal*, 56(7), 1242-1264.
23. Maxwell, R. M., & Miller, N. L. (2005). Development of a coupled land surface and groundwater model. *Journal of Hydrometeorology*, 6(3), 233–247.
24. Maxwell, R. M. (2013). A terrain-following grid transform and preconditioner for parallel, large-scale, integrated hydrologic modeling. *Advances in Water Resources*, 53, 109-117.
25. Maxwell, R. M., Condon, L. E., & Kollet, S. J. (2015). A high-resolution simulation of groundwater and surface water interactions in the continental United States. *Computers & Geosciences*, 85, 166–176.
26. Payne, W. A., Lascano, R. J., Wendt, C. W., & Ensor, P. L. (1991). Soil temperature and water under low-input conditions in Niger. *Agricultural and Forest Meteorology*, 57(1–3), 85–98.
27. Peugeot, C., Esteves, M., Galle, S., Rajot, J. L., Vandervaere, J. P., & Vieux, B. E. (1997). Runoff generation processes: Results and analysis of field data collected at the East Central Supersite of HAPEX–Sahel. *Journal of Hydrology*, 188–189, 179–202.

28. Rockström, J., Jansson, P., Barron, J., 1998. Seasonal rainfall partitioning under runoff and runoff conditions on sandy soil in Niger: on-farm measurements and water balance modelling. *Journal of Hydrology* 210, 68–92.
29. Simunek, J., Angulo-Jaramillo, R., Schaap, M.G., Vandervaere, J.P., van Genuchten, M.T., 1998. Using an inverse method to estimate the hydraulic properties of crusted soils from tension-disk infiltrometer data. *Geoderma* 86, 61–81.
30. Timouk, F. et al. (2009). Response of surface energy balance to monsoon variability over the Sahel. *J. Hydrol.*, 375, 56–66.
31. Vandervaere, J.P., Peugeot, C., Vauclin, M., Jaramillo, R.A., Lebel, T., 1997. Estimating hydraulic conductivity of crusted soils using disk infiltrometers and minitensiometers. *Journal of Hydrology* 188, 203–223.
32. Velluet, C., Demarty, J., Cappelaere, B., Braud, I., Viscel, T., Mougin, E., ... & Lloyd, C. R. (2014). Building a field- and model-based climatology of water and energy fluxes in the cultivated Sahel – annual budgets and seasonality. *Hydrology and Earth System Sciences*, 18, 5001–5024.
33. Velluet, C. (2014). *Modélisation et analyse pluriannuelles du fonctionnement hydrologique et énergétique de deux écosystèmes dominants au Sahel agropastoral (Sud-Ouest Niger)* (Doctoral dissertation, Université Montpellier II-Sciences et Techniques du Languedoc).